The defect microstructure of oxidized mantle olivine from Dish Hill, California

Jillian F. Banfield
Department of Geology and Geophysics, University of Wisconsin, Madison, Wisconsin 53706, U.S.A.

M. Darby Dyar
Department of Geological Sciences, University of Oregon, Eugene, Oregon 97403, U.S.A.

Anne V. McGuire
Department of Geological Sciences, University of Houston, Houston, Texas 77204, U.S.A.

Abstract

The defect microstructure and oxidation state of Fe in metasomatized olivine crystals from peridotite xenoliths from Dish Hill, California, have been studied by transmission electron microscopy (TEM) and Mössbauer spectroscopy. Previous petrographic studies suggested that these composite xenoliths were metasomatized under upper mantle conditions. Mössbauer data indicate that between 1 and 6% of the Fe in the olivine crystals is Fe^{3+}. TEM revealed the presence of layers 0.6 nm wide and parallel to (001) of olivine. The individual layers do not offset the surrounding olivine periodicities and are interpreted to be laihunite, an Fe^{3+} derivative of olivine, rather than humite-group minerals. The layers are found in (1) strong association with dislocations, with abundances decreasing rapidly with distance from the dislocation cores, (2) at grain boundaries, where layers of considerable length decrease in abundance with distance from the grain boundary, and (3) in local regions, where discontinuous layers, possibly formed by homogeneous nucleation, are evenly distributed throughout the olivine. These patterns suggest that the layers formed by alteration of olivine. TEM images from many areas revealed a very fine domain structure (~10 to 20 nm in diameter), possibly indicating short-range order of Fe^{3+} and vacancies. Some dislocations are associated with trails of submicrometer-sized fluid inclusions that contain iron oxide crystals a few tens of nanometers wide. These features may be healed fractures that provided pathways for oxidized Fe-bearing fluids. The association between laihunite and dislocations probably reflects the role of dislocations as rapid diffusion pathways and as sites for heterogeneous nucleation in olivine that is supersaturated with respect to Fe^{3+}. The subsequent reactivity, rheological, and transport properties of olivine may be modified substantially by laihunite layers on dislocations and at grain boundaries.

Introduction

Recent studies of spatial variation in the oxidation state of the upper mantle (e.g., Wood and Virgo, 1989; Ballhaus et al., 1991) suggest that some regions may have f_{O_2} values up to 2 log units above that defined by the fayalite + magnetite + quartz buffer (FMQ). Specifically, depleted regions that have experienced extensive mantle metasomatism and contain Ti- and Mn-enriched chromites, abundant phlogopite, and potassium richterite have oxidation states substantially above FMQ (Reid et al., 1975; Jones et al., 1983; Dawson and Smith, 1988; Winterburn et al., 1990). Mattioli et al. (1989) correlated f_{O_2} and major and trace element compositions in spinel peridotites and concluded that metasomatized peridotites were oxidized relative to unmetasomatized peridotites. The general coupling between mantle metasomatism and oxidation and the implications for the secular variation of f_{O_2} in the Earth are discussed by Ballhaus et al. (1991).

Evidence for metasomatism and oxidation can be found in the mineral content and microstructure of mantle-derived xenoliths. For example, Kitamura et al. (1987) reported that mantle olivine from a kimberlite contained planar defects parallel to (001) and {021}. On the basis of the displacement vector associated with the defects, the orientation of the defects, the offset of olivine periodicities, and the infrared absorption spectra, they suggested that these defects contain an OH-bearing monolayer, which, together with olivine slabs, can be described as humite-type interstratifications. Similarly, Drury (1991) described hydrated olivine from metamorphosed mantle-derived peridotite that contained $b = [001]$ dislocations that were commonly dissociated into widely separated partial dislocations, probably with $b = \langle 0 \ ^3/_{11} \ ^1/_4 \rangle$, and associated stacking faults. Drury noted the association between fluid inclusions and dislocations. He inferred that the planar defects are saturated with volatiles and rep-

resent humite-type interstratifications that grow into olivine by H^+ addition and dislocation climb.

Laihunite [ideally $Fe^{2+}Fe_2^{3+}(SiO_4)_2$] has been described as a low-pressure and low-temperature oxidation product of fayalite from numerous localities (see references in Banfield et al., 1990), and structural models based on vacancy ordering patterns have been proposed for several superstructures (Tamada et al., 1983; Shen et al., 1986). Laihunite has also been described in Mg-rich olivines from basaltic andesites (Banfield et al., 1990) and can be inferred to be present in the samples described by Kohlstedt and Vander Sande (1975). Laihunite has also been produced experimentally in olivines with a variety of compositions (Bartels and Burns, 1986, 1989; Kondoh et al., 1985; Iishi et al., 1989a, 1989b). However, the natural development of this mineral in mantle-derived olivine has not been reported.

A detailed study of the petrology of xenoliths from Dish Hill, California, demonstrated that metasomatic reaction between the peridotite and fluids derived from mantle dikes resulted in substantial increase in Fe^{3+}/Fe_{tot} relative to unmetasomatized peridotites (McGuire et al., 1991). These authors suggested that the metasomatic process involved addition of Fe^{3+} to existing minerals. The study described here was undertaken in order to test the hypothesis that laihunite was present within the olivine, to examine the distribution and structure of Fe^{3+}-bearing alteration products, and to determine whether humite-type interstratifications or other hydration and oxidation products were present.

SAMPLING AND EXPERIMENTAL METHODS

Results are reported from two xenolith samples from the Dish Hill cinder cone from the Deadman Lake Volcanic Field, California. Extensive compositional and petrographic data have been reported for the first sample, Ba-2-1, by Neilson and Noller (1987), Neilson et al. (1987), Wilshire et al. (1980, 1988), and McGuire et al. (1991). The petrographic relations and mineral compositions of the second sample, DH101, have been described by McGuire et al. (1991). Both samples have an amphibole-apatite-phlogopite dike remnant at one end. Olivine crystals hand-picked from both samples vary in color from clear green to greenish brown.

Polarized infrared spectroscopy

Infrared OH absorption spectra were obtained by George Rossman on a Nicolet 60SX Fourier transform IR spectrophotometer that uses a Michelson interferometer calibrated with a He-Ne laser. Further experimental details are reported by Miller et al. (1987).

Mössbauer spectroscopy

Olivine crystals examined by Mössbauer spectroscopy were coated with sugar under acetone to avoid preferred orientation, mounted in a Plexiglas holder with a diameter of approximately $^{15}/_{16}$ in., which corresponds to the area of the window on the detector, and exposed to the γ-ray flux. A ^{57}Co source ranging in strength from 10 to 25 mCi was used on an Austin Science Associates constant acceleration spectrometer. Base line counts from 6 to 60×10^6 were accumulated over long experiment times of up to one week. A gradient of approximately 0.018 359 mm/s/channel was employed to optimize spectral velocity resolution.

Spectra were fitted using a version of the program Stone modified to run on IBM and compatible personal computers. The program uses nonlinear regression procedures with a facility for constraining any set of parameters or linear combination of parameters. Lorentzian line shapes were used for resolving peaks, as there was no statistical justification for the addition of a Gaussian component to the peak shapes. Fitting procedures in general followed those described in Dyar et al. (1989) and McGuire et al. (1989).

The statistical quality of each fit was evaluated using the χ^2 and misfit parameters described in Ruby (1973). The value for percent misfit and its related percent uncertainty often appear as 0.00 in the tables; a percent misfit value of less than 0.01 indicates that the statistical error of the fitting procedure is less than that from the uncertainty of the data themselves, so that its actual value is not significant. The uncertainty of the Mössbauer data has been shown to be at best ± 0.02 mm/s for both isomer shift and quadrupole splitting and $\pm 1.5\%$ per peak for area (Dyar, 1984). This equates to $\pm 3\%$ of total Fe.

Transmission electron microscopy

Hand-picked olivine crystals from xenolith Ba-2-1 were mounted in epoxy. Thin sections of this composite were mounted on glass slides using a thermoplastic cement. Slices approximately 30 μm thick were removed from these sections and thinned to electron transparency by Ar ion milling in a liquid N_2–cooled ion mill.

A thin section perpendicular to the dike margin was prepared from xenolith DH101. Over 40 Cu grids (3 mm in diameter) were glued to the section, and slices were removed for ion milling. Approximately 15 oriented specimens from a sequence across the sample from the dike to the xenolith margin (corresponding with zones B–E in Fig. 1 of McGuire et al., 1991) were examined in the TEM.

Studies of the distribution of dislocations, alteration, and defect microstructure of olivine employed a JEOL 200-CX and a Philips 400T side-entry transmission electron microscope (TEM). Both of these microscopes are fitted with energy dispersive X-ray detectors, which allowed composition of minerals to be established. Additional high-resolution electron micrographs were recorded on a 200-kV CM-20 Ultratwin (Philips Electronics Application Laboratory, Eindhoven, the Netherlands).

RESULTS

Infrared spectroscopy

The polarized infrared absorption spectrum from the Dish Hill olivine exhibits only very weak bands (not

TABLE 1. Olivine compositions and Mössbauer data

	Ba-2-1					DH101			
	WR-1	WR-2	WR-3	WR-4	WR-5	B	C	D	E
SiO_2	39.00	39.40	39.40	40.20	39.80	40.48	40.91	41.10	41.10
TiO_2	na	na	na	na	na	0.00	0.00	0.01	0.01
Al_2O_3	na	na	na	na	na	0.00	0.01	0.02	0.01
Cr_2O_3	na	na	na	na	na	0.02	0.02	0.01	0.02
FeO	15.10	12.60	12.45	10.80	10.50	12.02	10.05	8.73	8.82
MnO	0.28	0.19	0.20	0.13	0.15	0.23	0.18	0.14	0.12
MgO	45.20	47.10	47.30	49.00	48.80	47.03	49.10	50.33	50.22
CaO	0.13	0.12	0.14	0.09	0.15	0.08	0.07	0.06	0.07
Na_2O	na	na	na	na	na	0.03	0.00	0.00	0.01
NiO	0.15	0.16	0.18	0.18	0.18	0.33	0.34	0.43	0.37
Sum	99.86	99.57	99.67	100.40	99.58	100.22	100.68	100.83	100.66
				Mössbauer parameters, two doublet fits					
δFe^{2+}	1.16	1.17	1.16	1.17	1.16	1.14	1.14	1.14	1.14
ΔFe^{2+}	2.97	2.98	2.98	2.98	2.98	2.98	2.98	2.98	2.98
ΓFe^{2+}	0.38	0.28	0.28	0.30	0.28	0.29	0.28	0.28	0.32
Area Fe^{2+}	99	98	97	99	98	97	96	96	94
δFe^{3+}_{oct}	0.45	0.44	0.45	0.45	0.44	0.45	0.48	0.44	0.43
ΔFe^{3+}_{oct}	0.73	0.70	0.73	0.73	0.71	0.67	0.61	0.67	0.68
ΓFe^{3+}_{oct}	0.29	0.25	0.26	0.31	0.26	0.31	0.38	0.42	0.32
Area Fe^{3+}_{oct}	1	2	3	1	2	3	4	4	6
% misfit	0.09	0.13	0.23	0.25	0.26	0.17	0.23	0.25	0.18
% uncertainty	0.01	0.02	0.01	0.01	0.01	0.01	0.01	0.01	0.01
				Mössbauer parameters, three doublet fits					
δFe^{2+}_{M1}	1.17	1.18	1.17	1.17	1.17	1.15	1.15	1.15	1.16
ΔFe^{2+}_{M1}	3.07	3.08	3.09	3.09	3.08	3.08	3.07	3.08	3.08
ΓFe^{2+}_{M1}	0.34	0.22	0.22	0.24	0.23	0.24	0.23	0.23	0.21
Area Fe^{2+}_{M1}	55	44	43	48	47	48	49	46	30
δFe^{2+}_{M2}	1.15	1.16	1.16	1.16	1.16	1.14	1.13	1.13	1.13
ΔFe^{2+}_{M2}	2.83	2.89	2.89	2.88	2.88	2.87	2.87	2.09	2.91
ΓFe^{2+}_{M2}	0.33	0.25	0.25	0.25	0.24	0.24	0.24	0.24	0.28
Area Fe^{2+}_{M2}	42	53	53	50	50	48	46	49	64
δFe^{3+}_{oct}	0.51	0.46	0.45	0.51	0.44	0.42	0.42	0.43	0.43
ΔFe^{3+}_{oct}	0.43	0.64	0.73	0.52	0.68	0.71	0.70	0.67	0.69
ΓFe^{3+}_{oct}	0.41	0.27	0.27	0.28	0.30	0.27	0.35	0.38	0.31
Area Fe^{3+}_{oct}	1	3	4	2	3	4	5	5	6
% misfit	−0.02	−0.02	−0.01	0.02	0.02	−0.02	−0.01	−0.01	−0.01
% uncertainty	0.00	−0.01	0.00	0.00	0.00	0.00	0.00	0.00	0.00
				Cations per formula unit					
Si	0.984	0.985	0.983	0.987	0.985	1.000	0.997	0.995	0.994
Ti	na	na	na	na	na	0.000	0.000	0.000	0.000
Al	na	na	na	na	na	0.000	0.000	0.001	0.000
Cr	na	na	na	na	na	0.000	0.000	0.002	0.000
Fe^{3+}	0.003	0.005	0.008	0.002	0.004	0.007	0.008	0.007	0.011
Fe^{2+}	0.315	0.258	0.252	0.220	0.213	0.241	0.197	0.170	0.168
Mn	0.006	0.004	0.004	0.003	0.003	0.005	0.004	0.003	0.002
Mg	1.700	1.754	1.759	1.794	1.800	1.733	1.784	1.816	1.813
Ca	0.004	0.003	0.004	0.002	0.004	0.002	0.002	0.002	0.002
Na	na	na	na	na	na	0.001	0.000	0.000	0.000
Ni	0.003	0.003	0.004	0.004	0.004	0.007	0.007	0.008	0.007
Sum	3.015	3.013	3.013	3.012	3.013	2.997	2.999	3.004	2.999

Note: Mössbauer parameters are given in millimeters per second for Γ (peak width), δ (isomer shift), and Δ (quadrupole splitting); the latter two parameters are relative to a metallic Fe foil calibration. Areas are given in percent of the total Fe present. Misfit and uncertainty parameters are given as defined by Ruby (1973). Cations per formula unit calculated using Fe^{3+} contents determined by three doublet fits and on the basis of four O atoms.

clearly distinct from the noise level) in the region of 3600 cm^{-1}, which is the expected position for OH vibrations in olivine minerals (G. Rossman, written communication, 1992). By comparison, spectra from clinohumite display a prominent sharp band near 3570 cm^{-1}. The absorbance measured for the sample of olivine from this study was 0.35, corresponding to a maximum of roughly 56–76 ppb OH. Comparison with Figure 1 of Miller et al. (1987) indicates that the Dish Hill samples are comparable to the most anhydrous of the olivine crystals analyzed in that study (George Rossman, personal communication, 1991).

Mössbauer spectroscopy

Mössbauer spectra were fitted with two doublet fits corresponding to Fe^{2+} and Fe^{3+} in octahedral sites (Fig. 1; Table 1), and these results were used to recalculate the olivine formulas presented there. The results reveal that between 1 and 6 ($\pm$ 3)% of the total Fe in the sample is Fe^{3+}; a preference for Fe^{3+} in either the M1 or M2 site of
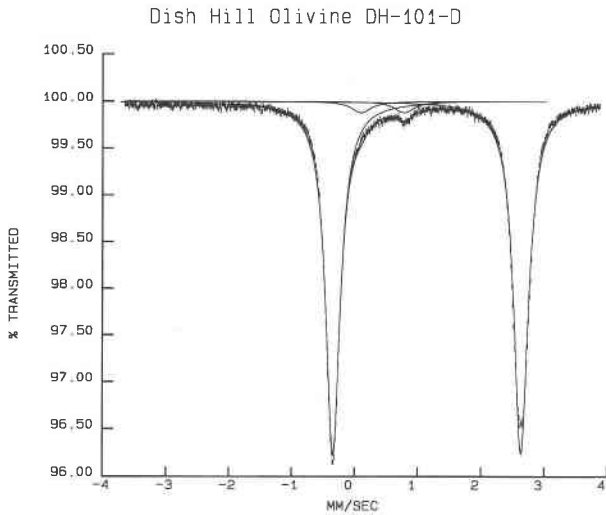
Dish Hill Olivine DH-101-D

Fig. 1. Mössbauer spectrum (two doublet fit) of olivine from DH101-D. Note the presence of the upper velocity peak of the Fe^{3+} doublet. Compositional data for this sample are provided in Table 1.

the structure could not be resolved. It should be noted that Schaefer (1985) concluded on the basis of infrared data that Fe^{3+} in "ferrifayalite" resides in the M2 site only. This may well be the case in the samples studied here; however, the resolution of the technique simply is not adequate to allow us to draw such a conclusion.

Additional fits utilizing three doublets were also performed to attempt to distinguish between Fe^{2+} in the M1 and M2 sites of the olivine structure. These two sites may well be distinguished by their differing point symmetries and geometrical distortions. The M1 octahedra share six of 12 edges and are tetragonally distorted (approximately D_{4h} symmetry), whereas the M2 octahedra share only three of 12 edges and are trigonally distorted (approximately C_{3v} symmetry). Because the sites are so dissimilar, it might be expected that Fe^{2+} and Mg would order into different sites. Recent studies by Ottonello et al. (1990) and Princivalle (1990) have demonstrated the dependence of cation ordering in these sites on composition, temperature, and (to a minor degree) f_{O_2}.

Parameters for the three doublet fits are also given in Table 1. Note that the statistical parameters of these fits are improved over the two doublet fits (in part simply because of the existence of more peaks in the model), but some peak widths are very close to their lower limits (0.21–0.25 mm/s). In general, the spectra show that Fe^{2+} is also disordered between the two sites, although sample DH101-E shows some indication of ordering into M2. However, the three doublet fits must be viewed with suspicion because the two Fe^{2+} doublets are highly overlapped in our room-temperature spectrum. High-temperature spectra will be needed to resolve the two Fe^{2+} doublets effectively; however, their resolution does not affect the amount of Fe^{3+} observed (within the known errors).
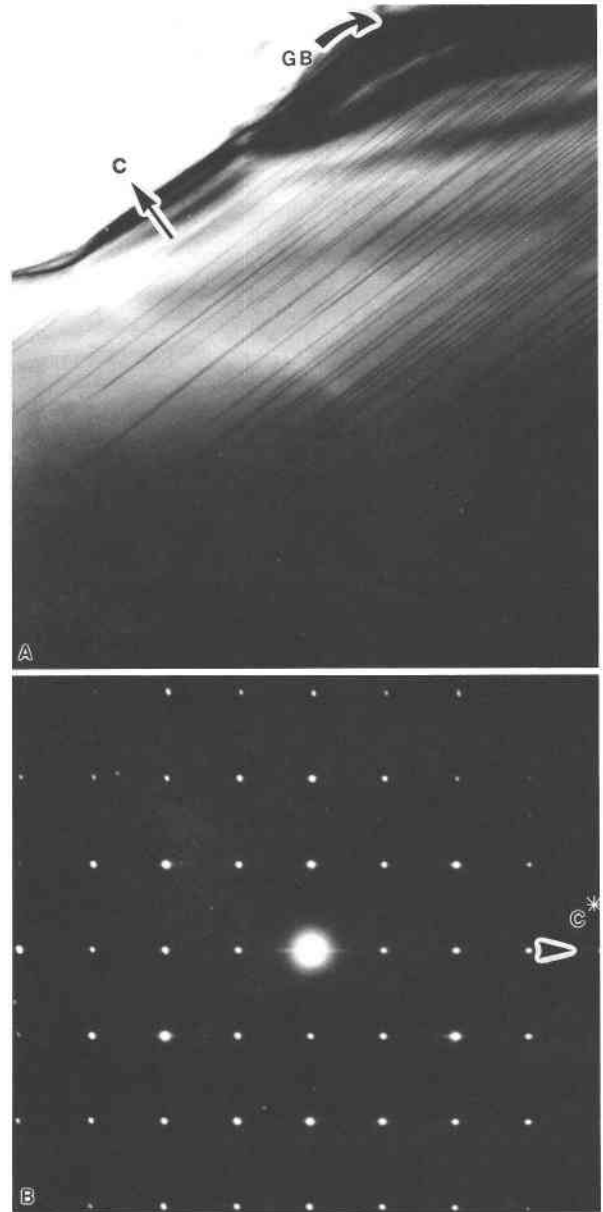

Fig. 2. (A) Transmission electron micrograph of olivine showing 0.6-nm wide layers parallel to (001) extending into the crystal from the grain boundary; (B) a [110] zone-axis selected-area electron diffraction pattern showing extensive streaking parallel to [001].

TEM

Electron microscopic observations from both the mounted olivine from Ba-2-1 and the DH101 xenolith thin section revealed the presence of layers parallel to (001) of olivine. Under appropriate conditions, elongate strips parallel to (001) olivine exhibit strong diffraction contrast. In lattice fringe images it is apparent that the strongly diffracting regions correspond to layers with the approximate c-axis dimension of olivine. In both samples these layers are very heterogeneous in distribution, with a strong association between abundant layers and grain
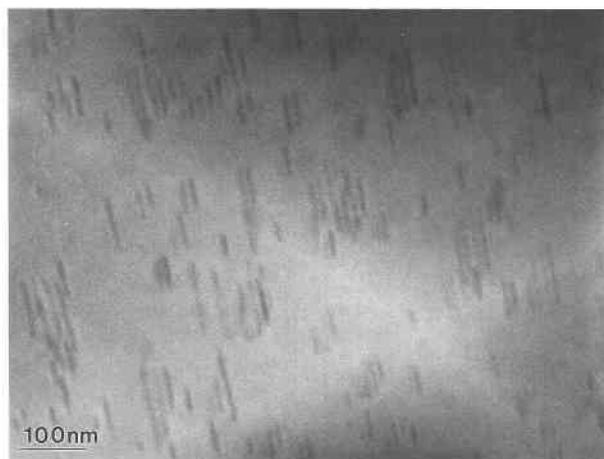
Fig. 3. Discontinuous layers parallel to (001) olivine showing no association with dislocations or a grain boundary.
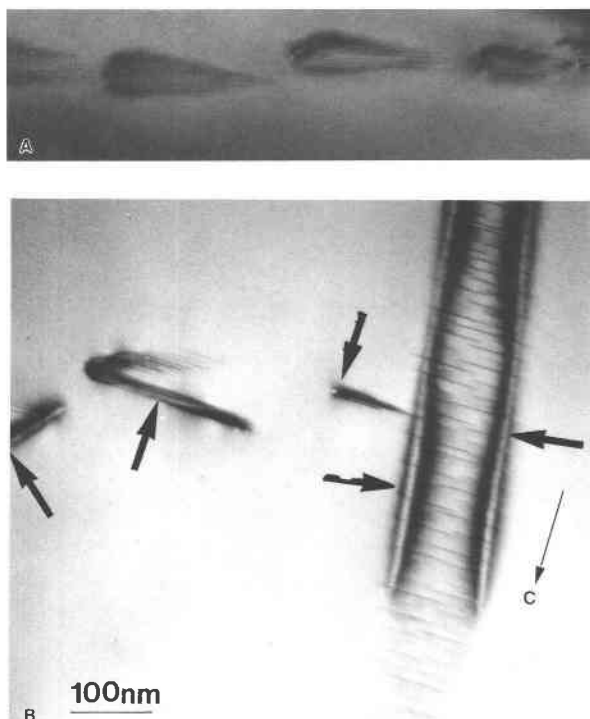

Fig. 5. (A) An area of olivine showing pronounced consistent asymmetry in the distribution of layers on dislocations (tear drop–shaped groups average 100 nm in length); (B) an area showing a variable asymmetrical distribution of layers on dislocations.

boundaries (Fig. 2A). Electron diffraction patterns illustrate pronounced streaking parallel to [001] (Fig. 2B). In general, the abundance of these planar layers decreases from every few unit cells at the grain boundary to every few hundred unit cells at a few tenths of a micrometer from the boundary.

Some areas of the samples contain numerous short layers distributed evenly throughout the olivine host. These areas are also commonly located near grain boundaries (Fig. 3). However, within the olivine crystals the most commonly occurring distribution pattern involves association with dislocations. In some areas the dislocations are free of these layers, and in other regions virtually all of the dislocations are "decorated" with layers that extend into the surrounding olivine (Fig. 4). The distribution of layers around the dislocations often shows a pronounced asymmetry. In some cases the asymmetry is consistent over large areas of the sample; in some cases it is not (Figs. 5A, 5B). In all cases the abundance of the layers decreases rapidly away from the dislocation cores.

Analysis of diffraction contrast in TEM images indicated that straight edge and screw dislocations with $\mathbf{b} =$ [001] are very common. The more highly curved sections of the dislocations appear to be most effective at pro-

moting the development of the layers (see Figs. 4, 5). Stacking faults associated with the dissociation of dislocations into partial dislocations with $\mathbf{b} \sim \langle 0\ \frac{1}{4}\ \frac{1}{4} \rangle$ reported in humite-bearing olivine were not observed.

The high-resolution electron micrograph in Figure 6 illustrates that the individual layers parallel to (001) of olivine have a dimension parallel to [001] olivine. These unit cells do not offset the surrounding olivine periodicities and thus have a spacing parallel to [001] olivine that is approximately equal to that of olivine (0.6 nm). This observation distinguishes the layers reported here from those described by Kitamura et al. (1987), which offset the surrounding periodicities and have a spacing that is clearly larger than that of olivine.

Despite the probable small dimensional difference parallel to [001] between the olivine and intergrown layers, there are no partial dislocations associated with the termination of the layer in Figure 6 (i.e., $\mathbf{b} = 0$). The structure of material within the layer (unit cell with distinct contrast) in Figure 6 is apparently continuous with that of the surrounding olivine. The small dimensional difference is due to compositional change and vacancies in an olivine-derivative structure and not to the termination of a structural layer. Our description of the termination of laihunite unit cells (e.g., without a very small partial dislocation) is consistent, for example, with the way in which we would view dimensional change in spinoidal decomposition (and in contrast to the description of the termi-

Fig. 4. An area of an olivine crystal containing abundant dislocations that are decorated by layers parallel to (001) olivine.
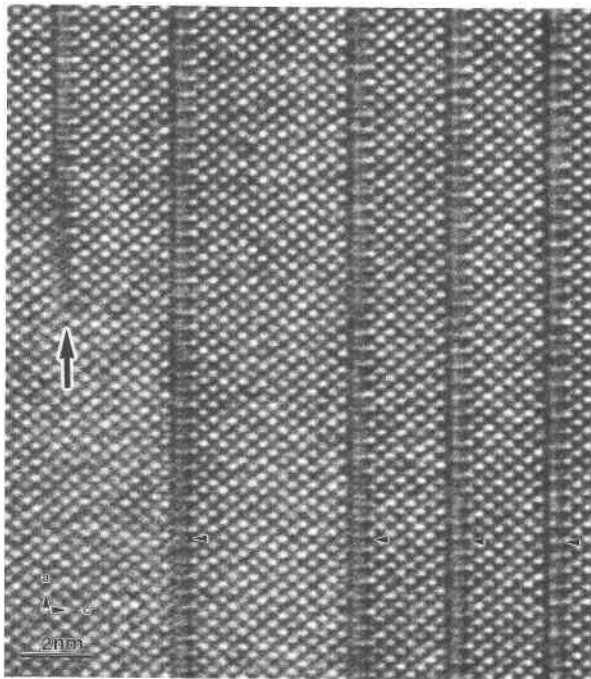
Fig. 6. A [010] zone-axis high-resolution transmission electron micrograph illustrating laihunite layers in olivine. Note the terminating layer passes smoothly into olivine (arrow).
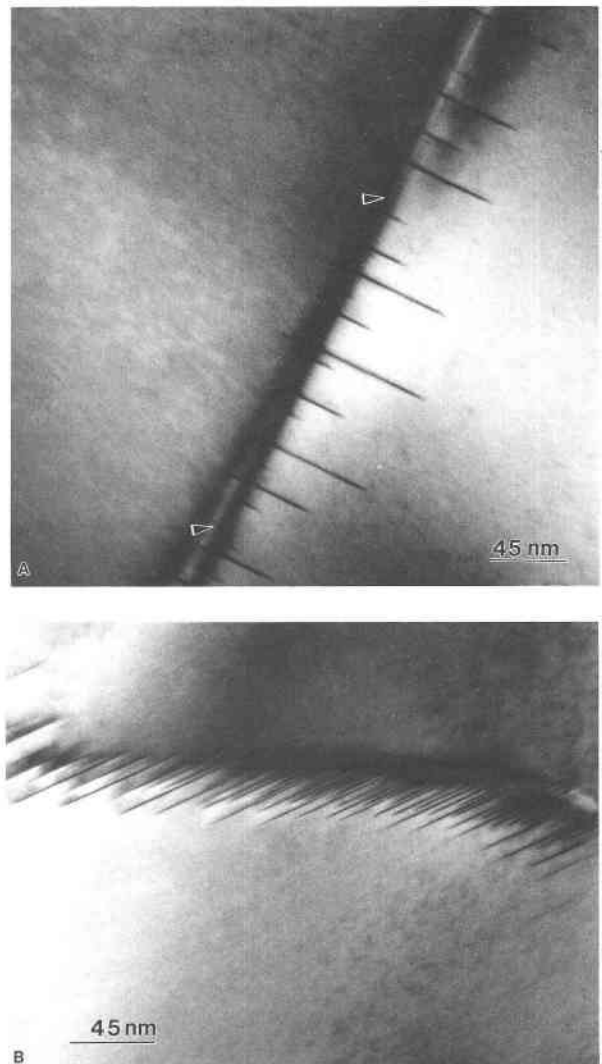

Fig. 7. (A) Darkfield and (B) brightfield transmission electron micrographs showing mottled areas surrounding dislocations decorated by laihunite layers. The mottling is suggestive of short-range order, possibly involving Fe^{3+} and vacancies.

nation of the hydroxide-rich humite interlayer at a partial dislocation in olivine).

When areas of olivine that contain occasional layers are exposed to a high electron dose during TEM examination, the beam damage is focused between the layers and not at the margins of the planar defects, as might be expected. This could indicate that the linear domains of material are compositionally distinct and are possibly more Fe rich. This compositional difference may explain the apparently reduced rate of ionization damage compared with the bulk material.

Oriented specimens were removed for TEM characterization from a pair of thin sections that represented an almost complete sequence from the dike margin across the entire xenolith. No systematic pattern involving higher (or lower) abundances of layers as a function of distance from the dike margin was detected. However, the abundance of the layers varied dramatically within the crystals. The sample that appeared to have the highest abundance of layers on average was obtained from approximately halfway between the margins.

TEM images, particularly darkfield images, from some regions display a pronounced mottled texture. This is generally only apparent when the sample is in a near two-beam condition or in weakly diffracting condition. The scale of the mottling is a few tens of nanometers (Fig. 7) and varies in prominence from one area to the next.

Figure 8 illustrates that some dislocations have series of fluid inclusions associated with them. These inclusions

commonly contain small (10 nm in diameter) oriented iron oxide crystals that have diffraction patterns consistent with magnetite.

None of the samples examined contains layers parallel to {021}, as would be expected for humite-type interstratifications. Furthermore, pyroxene, amorphous silica, magnetite, and hematite precipitates were not detected. However, sample DH101 did show signs of late-stage alteration. Occasional aggregates of smectite and iron oxides or hydroxides concentrated in channels at crystal margins were probably produced by surficial weathering. No correlation could be detected between boundaries showing this style of alteration and those exhibiting concentrations of the planar layers described above.
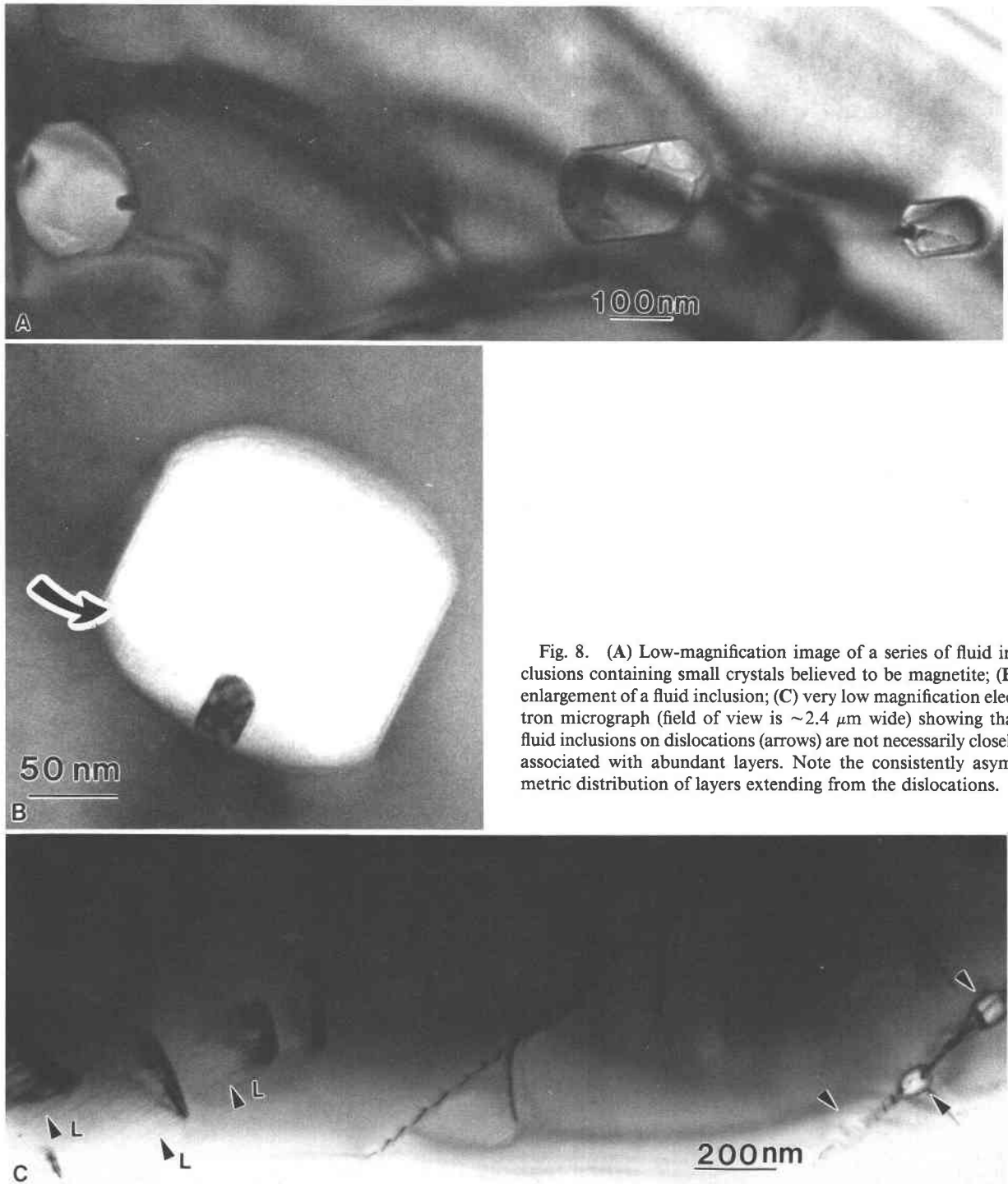
Fig. 8. (A) Low-magnification image of a series of fluid inclusions containing small crystals believed to be magnetite; (B) enlargement of a fluid inclusion; (C) very low magnification electron micrograph (field of view is ~2.4 μm wide) showing that fluid inclusions on dislocations (arrows) are not necessarily closely associated with abundant layers. Note the consistently asymmetric distribution of layers extending from the dislocations.

DISCUSSION

TEM observations have revealed that Fe^{3+}-bearing olivine crystals from metasomatized mantle xenoliths contain heterogeneously distributed individual layers of a mineral that is interpreted to be laihunite. The mode of occurrence of the laihunite as strips one unit cell wide parallel to (001) olivine closely resembles that of layers of OH-bearing humite-type interstratifications, as reported in previous studies. The distinction between laihunite and humite is made on the basis of the (001) interplanar spacing, the nature of the layer terminations, and the ab-

sence of the characteristic {021} layers. This interpretation is supported by the notable Fe^{3+} content revealed by Mössbauer analysis and the very low OH content as determined by infrared spectroscopy.

Figures 2, 3, 4, 5, and 7 illustrate three distinctive styles of laihunite distribution in olivine and reveal that these Fe^{3+}-bearing olivine-like layers are developed throughout the olivine crystals. The association of layers with both grain boundaries and dislocations is interpreted to reflect access to fast diffusion pathways. Based on compositional changes in the peridotite xenoliths and comparison with unmetasomatized xenoliths, McGuire et al. (1991) suggested that metasomatism involved addition of Fe^{3+} to existing minerals. However, the observations reported here seem more consistent with modification of the olivine by oxidation of structural Fe (with some Fe or Mg redistribution to maintain charge balance) rather than overgrowth or addition of Fe^{3+}-bearing material.

The distribution of laihunite in the mantle xenoliths differs from that in olivine from the andesitic lavas (Banfield et al., 1990). Only in the xenolith samples do we observe a pronounced concentration of layers around dislocation structures. Layers of laihunite are commonly developed in a consistent asymmetric pattern around the dislocations, with higher abundances frequently associated with the more curved parts of the dislocations. The explanation for the asymmetry is not clear.

Inclusion trails present within the olivine may represent healed fractures. The presence of iron oxide crystals within these inclusions and their association with dislocations suggest the passage of oxidized Fe-bearing fluids. The absence of intergrowths that could be identified as humite-type interstratifications, despite the indication that a hydrous fluid was present during alteration, may be explained if the alteration event took place under conditions that were not within the humite stability field.

Laihunite is present in olivine crystals from rocks that were subject to a thorough petrographic analysis that concluded that the assemblage formed in a mantle metasomatic event (McGuire et al., 1991). Because other parageneses for laihunite involve relatively low-temperature subsolidus oxidation, we must also consider this to be a possible explanation for the origin of laihunite in mantle xenoliths.

We do not dispute the conclusions of previous authors that laihunite formed at relatively low temperatures and pressures. However, we consider the possibility that laihunite may also be formed under higher temperature and pressure conditions. Pressure may extend the stability field of laihunite to higher temperatures. Because the volume of the unit cell of laihunite is about 2% smaller than that of forsterite and about 8% smaller than that of fayalite, pressure may favor segregation of randomly distributed Fe^{3+} and vacancies into laihunite layers.

Calculations by McGuire et al. (1991) indicate that for an olivine grain with a 2-mm radius at 1300 °C and an f_{O_2} at QFM, a period of approximately 10 yr would be required to homogenize the Fe and longer for O. This result suggests that diffusion rates are sufficiently fast to preclude the long-term preservation of the observed textures at upper mantle conditions. Similarly, diffusion rates are probably too slow to allow appreciable redistribution of cations and O during the few hours-to-weeks time scale of transport of the xenoliths to the surface and their subsequent eruption in the cinder cone. We suggest that the oxidation-metasomatic event may have occurred in the mantle immediately prior to eruption.

As well as providing diffusion pathways, the dislocations provided nucleation sites for laihunite. However, a homogeneous nucleation process in olivine saturated with Fe^{3+} is suggested in some areas by short, regularly spaced layers (Fig. 3) with no direct association with dislocations or grain boundaries. The mottling in darkfield and other images (e.g., Fig. 7) suggests the development of regions exhibiting short-range order, possibly of Fe^{3+} and vacancies. Cation and vacancy ordering may be a precursor stage for growth of laihunite.

Laihunite is an Fe^{3+}-bearing olivine-derivative structure in which charge balance is achieved by creation of octahedral vacancies; e.g., $(Fe^{3+}_x Fe^{2+}_{1-x}, Mg_x)_{\sim 1.6}SiO_4$. At this stage in our investigations we have not been able to establish how much Mg is incorporated into the laihunite structure. The laihunite unit cells may contain virtually no Mg (as in laihunite as originally described), with Mg partitioning strongly into coexisting forsterite-rich olivine. Alternatively, the laihunite may contain appreciable Mg. These issues were discussed by Banfield et al. (1990) and remain unresolved.

The formation of laihunite clearly indicates an episode involving modified redox conditions. We believe that the oxidation event involved an increase in f_{O_2} rather than the lowering of f_{H_2}. The diffusive loss of H during ascent, coupled with oxidation of Fe, has been suggested by Dyar et al. (1992) to explain a near perfect inverse relation between H^+ and Fe^{3+} content in kaersutite amphiboles. If such a process were responsible for the Fe^{3+} content of olivine, the OH content of the original mantle material would have been extraordinary (i.e., one H^+ for each Fe^{3+}). The distribution of the laihunite at dislocations (given rapid diffusion rates for H) also provides strong evidence to rule this out as the predominant oxidation mechanism. Thus, we interpret the Fe^{3+} content of olivine to reflect f_{O_2} greater than those of the olivine stability field. At least qualitatively, the distribution and concentration of the laihunite is considered to be an interesting indicator of submicroscopic f_{O_2} gradients within crystals.

It is clear that an f_{O_2} buffering reaction involving olivine and laihunite can be written; for example, Fe_2SiO_4 (olivine) + $0.2667O_2$ (fluid) → $Fe_{1.6}SiO_4$ (laihunite) + $0.1333Fe_3O_4$ (spinel). The lack of secondary iron oxide crystals in the olivine suggests that diffusion was sufficiently fast to allow the redistribution of Fe (and possibly Mg) into coexisting minerals. The usefulness of O buffering reactions such as this cannot be established until considerable progress is made toward understanding the composition of laihunite in forsterite-rich olivine, the sta-

bility field is examined by high-pressure, high-temperature experimentation, and the thermodynamic properties of laihunite are investigated.

At present we do not know whether laihunite is a stable or metastable phase under the conditions of its formation. The kinetics of a laihunite precipitation reaction may be favorable compared with diffusional loss of silica and growth of magnetite in the olivine matrix. Experimental work is currently in progress to explore this possibility.

We consider the question of a possible high-temperature, high-pressure (i.e., mantle metasomatic) origin for the laihunite to be an extremely important one. The unresolved question of the timing of the laihunite formation is of broader significance, given the not uncommon nature of relatively oxidized mantle rocks that have been interpreted to reflect relatively high mantle f_{O_2}. The growth of compositionally distinct layers may alter (enhance or retard) the subsequent movement of dislocations, thus modifying the rheology of the oxidized olivine-dominated rocks. The effect of the layers on the subsequent reactivity will be amplified by the concentration of the layers at reactive sites (dislocations and grain boundaries). Furthermore, the stability, thermodynamic properties, diffusion rates, elemental partitioning, melting temperature, and other properties of the olivine will be different from that of unaltered olivine. This may have important consequences for petrologic studies and for the many experimental investigations that use xenolith-derived olivine.

REFERENCES CITED

Ballhaus, C., Berry, R.F., and Green, D.H. (1991) High pressure experimental calibration of the olivine-orthopyroxene-spinel oxygen geobarometer: Implications for the oxidation state of the upper mantle. Contributions to Mineralogy and Petrology, 107, 27–40.

Banfield, J.F., Veblen, D.R., and Jones, B.F. (1990) Transmission electron microscopy of subsolidus oxidation and weathering of olivine. Contributions to Mineralogy and Petrology, 106, 110–123.

Bartels, K.S., and Burns, R.G. (1986) Structural Fe³⁺ induced in heated Mg-Fe and Mn-Fe olivines. Transactions of the American Geophysical Union, 44, 1270.

——— (1989) Heat oxidized olivines: Characterization of reaction products by 4.2 K Mössbauer spectroscopy. Twenty-eighth International Geological Congress Abstracts, 92–93.

Dawson, J.B., and Smith, J.V. (1988) Metasomatized and veined upper mantle xenoliths from Pello Hill, Tanzania: Evidence for anomalously-light mantle beneath the Tanzanian sector of the East African Rift Valley. Contributions to Mineralogy and Petrology, 100, 510–527.

Drury, M.R. (1991) Hydration-induced climb dissociation of dislocations in naturally deformed mantle olivine. Physics and Chemistry of Minerals, 18, 106–116.

Dyar, M.D. (1984) Precision and interlaboratory reproducibility of measurements of the Mössbauer effect in minerals. American Mineralogist, 69, 1127–1144.

Dyar, M.D., McGuire, A.V., and Ziegler, R.D. (1989) Redox equilibria and crystal chemistry of coexisting minerals from spinel lherzolite mantle xenoliths. American Mineralogist, 74, 969–980.

Dyar, M.D., McGuire, A.V., and Mackwell, S.J. (1992) Fe³⁺/H⁺ and D/H in kaersutites—Misleading indicators of mantle source fugacities. Geology, 20, 565–568.

Iishi, K., Kadomi, M., and Okamota, K. (1989a) Synthesis of laihunite by heating Fe-Mn olivine in air. Neues Jahrbuch für Mineralogie Monatshefte, 6, 245–254.

Iishi, K., Okamoto, K., and Kadomi, M. (1989b) Formation of laihunite from Fe-(Mg,Co,Mn,Ca) olivines. Neues Jahrbuch für Mineralogie Monatshefte, 8, 345–356.

Jones, A.P., Smith, J.V., and Dawson, J.B. (1983) Glasses in mantle xenoliths from Olmani, Tanzania. Journal of Geology, 91, 167–178.

Kitamura, M., Kondoh, S., Morimoto, N., Miller, G.H., Rossman, G.R., and Putnis, A. (1987) Planar OH-bearing defects in mantle olivine. Nature, 328, 143–145.

Kohlstedt, D.L., and Vander Sande, J.B. (1975) An electron microscopy study of naturally occurring oxidation produced precipitates in iron-bearing olivines. Contributions to Mineralogy and Petrology, 53, 13–24.

Kondoh, S., Kitamura, M., and Morimoto, N. (1985) Synthetic laihunite [$\square_x$ Fe²⁺₃₋ₓFe³⁺₂ₓSiO₄], an oxidation product of olivine. American Mineralogist, 70, 737–746.

Mattioli, G.S., Baker, M.B., Rutter, M.J., and Stolper, E.M. (1989) Upper mantle oxygen fugacity and its relationship to metasomatism. Journal of Geology, 97, 521–536.

McGuire, A.V., Dyar, M.D., and Ward, K.A. (1989) Neglected Fe³⁺/Fe²⁺ ratios—A study of Fe³⁺ content of megacrysts from alkali basalts. Geology, 17, 687–690.

McGuire, A.V., Dyar, M.D., and Nielson, J.E. (1991) Metasomatic oxidation of upper mantle peridotite. Contributions to Mineralogy and Petrology, 109, 252–264.

Miller, G.H., Rossman, G.R., and Harlow, G.E. (1987) The natural occurrence of hydroxide in olivine. Physics and Chemistry of Minerals, 14, 461–472.

Neilson, J.E., and Noller, J.S. (1987) Processes of mantle metasomatism; constraints from observations of composite peridotite xenoliths. Geological Society of American Special Paper 215, 61–76.

Neilson, J.E., Badahn, J.R., and Wilshire, H.G. (1987) Fractionation of REE in a composite xenolith, Dish Hill, California. Geological Society of America Abstracts with Programs, 19, 436–437.

Ottonello, G., Princivalle, F., and Della Giusta, A. (1990) Temperature, composition, and f_{O_2} effects on intersite distribution of Mg and Fe²⁺ in olivines. Physics and Chemistry of Minerals, 17, 301–312.

Princivalle, F. (1990) Influence of temperature and composition on Mg-Fe²⁺ intracrystalline distribution in olivines. Mineralogy and Petrology, 43, 121–129.

Reid, A.M., Donaldson, C.H., Brown, R.W., Ridley, W.I., and Dawson, J.B. (1975) Minerals chemistry of peridotite xenoliths from the Lashaine volcano, Tanzania. Physics and Chemistry of the Earth, 9, 525–543.

Ruby, S.L. (1973) Why misfit when you already have χ^2? In I.J. Gruverman, C.W. Seidel, and D.K. Dieterly, Eds., Mössbauer effect and methodology, vol. 9, p. 263–276. Plenum Press, New York.

Schaefer, M.W. (1985) Site occupancy and two-phase character of "ferrifayalite." American Mineralogist, 70, 729–736.

Shen, B., Tamada, O., Kitamura, M., and Morimoto, N. (1986) Superstructure of laihunite-3M [$\square_{0.4}$Fe²⁺₀.₈Fe³⁺₀.₈SiO₄]. American Mineralogist, 71, 1455–1460.

Tamada, O., Shen, B., and Morimoto, N. (1983) The crystal structure of laihunite [$\square_{0.4}$Fe²⁺₀.₈Fe³⁺₀.₈SiO₄]—A nonstoichiometric olivine-type mineral. Mineralogical Journal, 11, 382–391.

Wilshire, H.G., Neilson Pike, J.E., Meyer, C.E., and Schwarzman, E.C. (1980) Amphibole-rich veins in lherzolite xenoliths, Dish Hill and

Deadman Lake, California. American Journal of Science, 280A, 576–593.

Wilshire, H.G., Meyer, C.E., Nakata, J.K., Calk, L.C., Shervais, J.W., and Schwarzman, E.C. (1988) Mafic and ultramafic xenoliths from volcanic rocks of the western United States. U.S. Geological Survey Professional Paper 1443, 179 p.

Winterburn, P.A., Harte, B., and Gurney, J.J. (1990) Peridotite xenoliths from the Jagersfontein kimberlite pipe: I. Primary and primary metasomatic mineralogy. Geochimica et Cosmochimica Acta, 54, 329–341.

Wood, B.J., and Virgo, D. (1989) Upper mantle oxidation state: Ferric iron contents of lherzolite spinels by 57 Mössbauer spectroscopy and resultant oxygen fugacities. Geochimica et Cosmochimica Acta, 53, 1277–1291.